Robustness of Localized DNA Strand Displacement Cascades

Mario Teichmann,[†] Enzo Kopperger,[†] and Friedrich C. Simmel[†,‡,*]

[†]Physics Department E14 and ZNN/WSI, Technische Universität München, Garching 85748, Germany, and [‡]Nanosystems Initiative Munich, Munich 80799, Germany.
M.T. and F.C.S. designed the research, M.T. performed the experiments, M.T., E.K., F.C.S. analyzed the data, M.T., E.K., F.C.S. wrote the manuscript.

ABSTRACT Colocalization can strongly alter the kinetics and efficiency of chemical processes. For instance, in DNA-templated synthesis unfavorable reactions are sped up by placing reactants into close proximity onto a DNA scaffold. In biochemistry, clustering of enzymes has been demonstrated to enhance the reaction flux through some enzymatic cascades. Here we investigate the effect of colocalization on the performance of DNA strand displacement (DSD) reactions, an important class of reactions utilized in dynamic DNA nanotechnology. We study colocalization by immobilizing a two-stage DSD reaction cascade comprised of a "sender" and a "receiver" gate onto a DNA origami platform. The addition of a DNA (or RNA) input strand displaces a signal strand from the sender gate, which can then transfer to the receiver gate. The performance of the cascade is found to vary strongly with the distance between the gates. A cascade with an intermediate gate distance of ≈20 nm exhibits faster kinetics than those with larger distances, whereas a cascade with smaller distance is corrupted by excessive intraorigami leak reactions. The 20 nm cascade is found to be considerably more robust with respect to a competing reaction, and implementation of multiple receiver gates further increases this robustness. Our results indicate that for the 20 nm distance a fraction of signal strands is transferred locally to a receiver gate on the same platform, probably involving direct physical contact between the gates. The performance of the cascade is consistent with a simple model that takes "local" and "global" transfer processes into account.

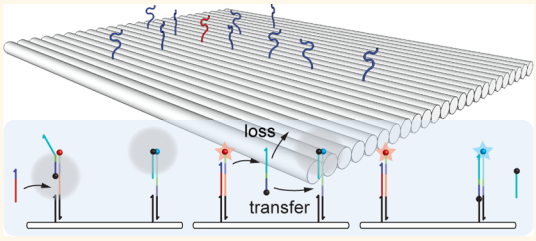

KEYWORDS: DNA nanotechnology · molecular programming · DNA strand displacement circuits · DNA origami · colocalization

DNA strand displacement (DSD) reactions are basic operations of dynamic DNA nanotechnology.[1] They typically involve three DNA strands—an input strand, an output strand, and a "gate" strand. Input and output strands are both partially complementary to the gate strand, but may be extended by additional sequences with other function. Initially, output and gate strands are hybridized to each other within gate complexes. Upon addition of a DNA input to a gate complex, the output strand is displaced from the gate strand in a branch migration process. Branch migration can be sped up considerably by utilization of "toehold" sequences, which are short single-stranded extensions of the gate complex at which an input strand can attach and initiate strand invasion.[2] The kinetics of DSD processes have been studied extensively both in experiment[3] and theory.[4] DSD reactions can be rationally "wired up" into circuits *via* sequence-addressable toeholds. The modular nature of the DSD components allows formal abstraction and has even resulted in the development of a high level molecular programming language for DSD circuits.[5]

DSD reactions have been previously used to drive a large variety of DNA-based nanomechanical devices through their operation cycles,[6] but they have also been utilized for DNA-based computation. For instance, DSD reactions have been used as the basis for molecular logic gates and circuits,[7,8] for the realization of catalytic and autocatalytic reaction networks,[9,10] and even for the demonstration of molecular neural network computation.[11] One particularly promising application for computational DNA-based reaction cascades is the realization of autonomous biosensing devices that process biological information *in situ*, *e.g.*, the analysis of disease-related microRNA (miRNA) patterns.[7,12,13]

Colocalization of DSD circuit components on supramolecular scaffolds is expected to be beneficial for their performance for a variety of reasons, which have been previously discussed in several theoretical studies.[14−16] Colocalization can increase the "local concentration" of reactants and

* Address correspondence to simmel@tum.de.

Received for review June 6, 2014 and accepted August 4, 2014.

Published online August 04, 2014
10.1021/nn503073p

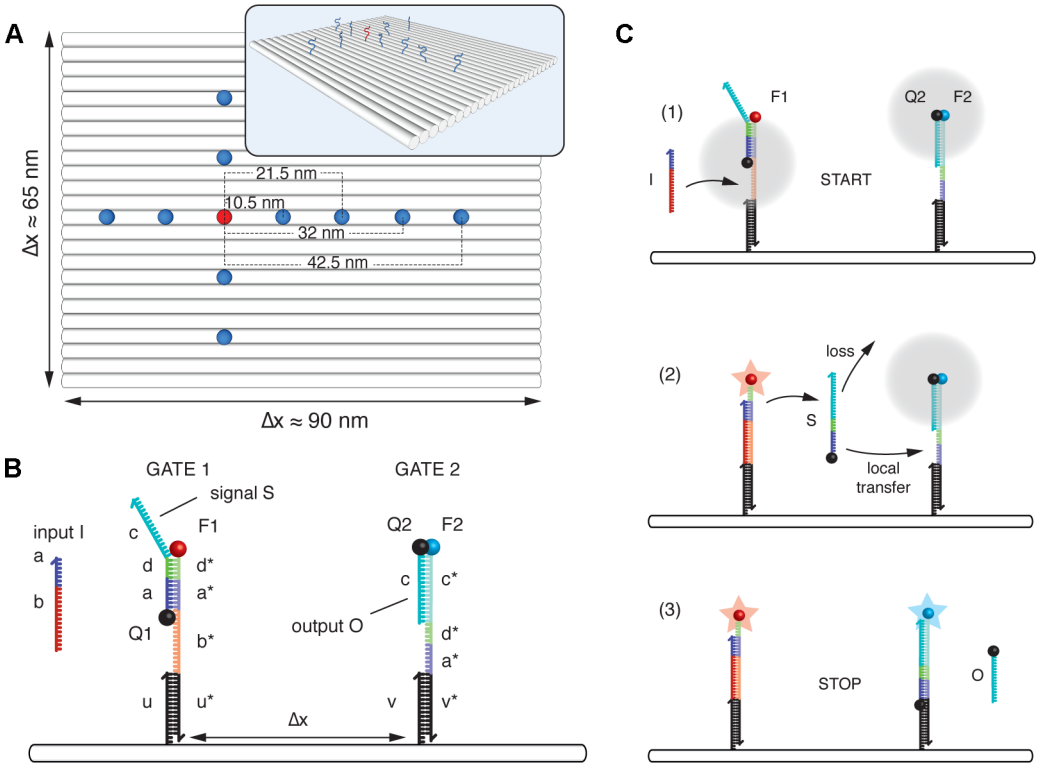

Figure 1. Schematic illustration of the immobilized DNA strand displacement cascade. (A) A rectangular single-layered DNA origami platform (dimensions ≈ 90 nm × 65 nm) is used to define the positions of the components of the DSD cascade. A DNA sender gate 1 is hybridized to an extended staple position at the position indicated in red. Extended staples for receiver gates (depicted in blue) can be placed at various distances from the sender as indicated. Inset: 3D perspective of the platform. (B) DNA strands and domains involved in the DSD cascade shown in its initial state. Sender gate 1 is hybridized to a staple extension with sequence domain u, receiver gate 2 is hybridized to a staple extension v at a distance Δx from the sender. The sequence domain lengths are a: 7 nt, b: 15 nt, c: 16 nt, d: 5 nt, u, v: 16 nt. For fluorescent readout, gate 1 and gate 2 are labeled with fluorophores F1 and F2, while signal and output strands carry fluorescence quenchers Q1 and Q2. (C) Progress of the reaction cascade. Addition of input strand I triggers the release of an intermediate signal strand S, which in turn displaces the "output" strand O. Release of S is accompanied by a fluorescence increase of F1, while release of O leads to an increase in fluorescence of F2.

thus speed up bimolecular reactions. Reduction of the loss of reaction intermediates by diffusion can increase the robustness of reactions with respect to external disturbances, and reduced crosstalk between spatially separated processes enables the reuse of identical circuit components and modules within a single system. In fact, similar roles for colocalization have been attributed to supramolecular assemblies in cellular biochemistry such as multienzyme complexes,[17] or signaling components such as G protein coupled receptors and scaffolded phosphorylation cascades. Colocalization of reactants on DNA supports has already been utilized in the context of DNA-templated synthesis,[18,19] and also for the realization of artificial enzyme cascades.[20−24]

As a model system we here study a simple two-stage DSD cascade, whose components are immobilized onto a DNA origami substrate (Figure 1A,B, Figure S1, Supporting Information (SI)). In this system, the addition of a DNA or RNA input strand triggers the release of an intermediate signal strand from the first gate of the cascade. The intermediate strand can activate a second gate on the origami platform and release an output strand in another strand displacement process (Figure 1C).

We find that the overall kinetics of the process is considerably sped up only for an intermediate spatial separation (≈ 21.5 nm) between the DSD stages, whereas colocalization does not have a significant effect for larger distances. At smaller distances (≈ 10.5 nm), direct physical overlap of the gates results in strong intraorigami leak reactions, which precludes a stable preparation of the DSD cascades. We demonstrate that for the smallest *stable* gate distance the DSD cascade is robust with respect to excessive amounts of interfering DNA strands that are partially sequence-complementary to the intermediate signal strand. A redundant architecture with four receiver gates on a single origami platform considerably improves the speed and robustness of the system.

RESULTS

Experimental Setting. Our experimental realization of the two-stage DSD cascade is schematically depicted in Figure 1. The platform for the cascade is based on a twist corrected rectangular origami structure

(modified from the literature[25]) with dimensions 90 nm × 65 nm (Figure 1A, for AFM imaging see Figure S1B (SI)). As indicated, some of the staple strands are extended with adaptor sequences to which the DSD gate strands are hybridized (*cf.* Figures S1 and S2 (SI)). The distance Δx between "sender" gate 1 and "receiver" gate 2 is varied in the experiments between 3, 6, 9, and 12 full helical turns (*i.e.*, nominally $\Delta x \approx 10.5$, 21.5, 32 and 42.5 nm). In addition, the stoichiometry between sender and receivers is varied for the smaller gate distances. We also considered a "diagonal" position at $\Delta x \approx 15$ nm (*cf.* Figure S1A (SI)), which was found to have similarly strong leakage as the 10.5 nm distance, and was thus not investigated further. In the initial state of the cascade, the sender gate is loaded with a signal strand S, and the receiver gate is hybridized to an output strand O. Both S and O carry fluorescence quencher molecules (Q1 and Q2, respectively), which quench the fluorescence of the fluorophores F1 and F2 on the gate strands. Upon addition of an input strand I signal strand S is released and displaces the strand O from gate 2 *via* toehold-mediated branch migration (Figure 1C). In principle, the "dummy"-output strand O could be extended by an additional output sequence in order to trigger downstream processes and thus serve as a "real" output. The architecture of the cascade is similar to that of previously developed toehold-exchange reactions.[3,10] The release of output may either occur on the same origami platform *via* local transfer of the signal S or on a different platform *via* interorigami diffusion. In order to feed the cascade with a "realistic" input (in terms of biosensing applications), the sequence of the input strand was chosen to be that of microRNA-21 (miR-21), a regulatory RNA molecule whose expression level is up-regulated in all human solid cancers.[26,27] This naturally occurring sequence is not optimized for the cascade and constrains the sequences for the rest of the design.

Assembly of the Cascade and Intraorigami Strand Exchange. Intrinsic to the nature of the strand displacement process, the repeated use of DNA subsequences is unavoidable. In the initial state of the cascade in Figure 1B, sequence domains a*, c and d* occur twice. We found that colocalization of the gates on the origami scaffold already results in considerable strand displacement leakage, in which signal strand S is transferred from gate 1 to gate 2 even in the absence of input I (Figure S3 (SI)). In order to reduce leakage during assembly of the cascade, we passivated the signal strands with auxiliary protection strands P (containing sequence domain c* and a toehold for deprotection, Figure S2 (SI)). Undesired gate interactions were strongly reduced by this passivation for intergate distances above 21.5 nm, but were still significant for the 10.5 nm distance (Figures S4 and S5 (SI)). The displacement of Q2 by I was explicitly excluded by the design of the sequences and was shown to have no impact on the fluorescence collected from F2 (Figure S6 (SI)).

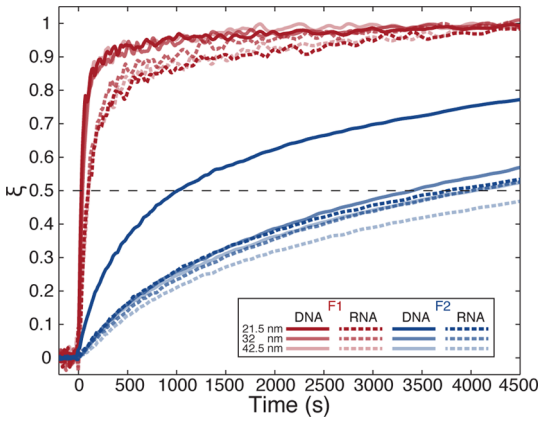

Figure 2. Progress of the cascade reaction with DNA and RNA inputs for distances $\Delta x \approx$ 21.5, 32, and 42.5 nm. Fluorescence of sender gate fluorophore F1 and the receiver fluorophore F2 (*cf.* Figure 1B,C) are shown for the various distances as indicated by the colors (see legend). Release of the signal strand from gate 1 (red traces) is ≈100 times faster than capture of the signal strands (blue traces), as input strands are added in 100 fold excess. The trace recorded for the $\Delta x \approx$ 21.5 nm gate distance for DNA inputs displays a fast initial phase, which may be interpreted as caused by a "local", intraorigami signal strand transfer.

In order to rationalize this observation, one has to consider the geometric dimensions of the various components of the cascade. In the initial state of gate 1, sequence domains u/u*, a/a* and d/d* are in a duplex conformation, while b* and c are single-stranded. In a relaxed conformation, a single-stranded DNA section of n nucleotides is assumed to have a typical "length" of $\approx (b_k l)^{1/2}$, where $b_k \approx 1.6$ nm is the Kuhn length of single-stranded DNA,[28,29] and $l = n \times 0.6$ nm is its contour length.[29] Considering also the dithymidine spacers between the origami platform and the gates, in a relaxed linear conformation the length of gate 1 is thus estimated to be ≈18.6 nm (in the protected state ≈20.1 nm), while gate 2 has length ≈15.6 nm. Fully stretched to their contour lengths, gate 1 and gate 2 have lengths ≈29.3 nm and ≈19.3 nm. Thus, already in a relaxed conformation, the two gates can physically interact at their "tips". At distances above ≈33 nm, however, the strand orientation of the signal strand S does not allow for a direct transfer to gate 2 *via*, *e.g.*, duplex fraying followed by strand displacement (*cf.* also Discussion and Figure 6).

Distance Dependence of Cascade Kinetics. As for the 10.5 nm gate distance proximity-induced intraorigami strand transfer prevented the preparation of a defined initial state that was stable on the time-scale of our experiments, we investigated the kinetics of the cascaded DSD reaction only for the larger distances $\Delta x \approx$ 21.5, 32, and 42.5 nm.

In Figure 2, the release kinetics of the intermediate strand and the final output strand is compared both for

DNA and RNA input molecules. For better comparison, all fluorescence traces were normalized to vary between a starting level ξ (t = 0) = 0 and an end level ξ ($t \rightarrow \infty$) = 1, where the fluorescence end levels were determined for each experiment individually (Figure S7 (SI)). Thus, ξ (t) represents the fractional progress of the displacement reactions. In fact, due to intraorigami leakage reactions the starting fluorescence levels varied slightly between the experiments, with higher starting levels for the F2 signal for the shorter gate distances (*cf.* Figure S8 (SI)).

In each case the cascade was first activated by removal of the protection strands P from gate 1, and then triggered by the addition of input strands in large excess ([*I*] $\approx$ 0.47 μM) over the origami platforms present at [*O*] $\approx$ 4.8 nM (Figure S5 (SI)). As expected, the kinetics of the signal release step is independent of the distance between sender and receiver. In fact, the corresponding fluorescence traces monitored by fluorophore F1 were almost identical throughout all of our experiments.

The kinetic curves could not be well fit with a simple rate law, but appeared to result from a superposition of several processes (and potentially contained contributions from several fluorescent species in different quenching states). As a rough measure of the reaction speed, we thus determined the half-times $t_{1/2}$ of the reactions (ξ ($t_{1/2}$) = 0.5), which were found to vary between 30 and 40 s for DNA inputs, and were close to 100 s for the RNA inputs. If we ignore the apparently more complicated release kinetics and relate the half-times to an effective second order rate constant $k_{on} = (c \cdot t_{1/2})^{-1}$ (with $c = [I]$), we obtain $k_{on} \approx 6 \times 10^4\ M^{-1}\ s^{-1}$ and $\approx 2 \times 10^4\ M^{-1}\ s^{-1}$ for DNA and RNA, respectively. This is in the lower range of typical hybridization reaction rates. One of the reasons for the relatively slow kinetics may be the presence of secondary structure in the miR-21 derived input strand, which has a folding free energy of -2.71 kcal/mol for the DNA input sequence, and even -5.31 kcal/mol for the RNA input.

The second step of the cascade involves the intermediate signal strand S, which triggers the release of the output strand O carrying quencher Q2, and thus results in an increase of the fluorescence of fluorophore F2. In contrast to the first step, the signaling step appears to be sensitive to the distance between the gates. For the DNA input, the 21.5 nm gate distance clearly resulted in faster overall kinetics ($t_{1/2}$ = 1000 s) than the larger distances (32 and 42.5 nm), for which the kinetics were quite similar ($t_{1/2}$ = 3410 s and 4010 s). Interestingly, for the RNA input, all three distances resulted in similarly slow reactions with half-times $t_{1/2}$ = 3770, 4000, 5000 s for 21.5, 32, 42.5 nm, respectively.

The ratio of $\approx$100 between half-times for the slow signaling reactions (*i.e.*, all but the DNA input/Δx = 21.5 nm case) and the release step corresponds very well to the concentration ratio between input and signal strands ([*I*]/[*O*] = 0.47 μM/4.8 nM $\approx$ 100). This strongly suggests that in these cases the intermediate signal strands are not transferred "locally" on the origami platforms, but are first released to the bulk, and then return to the output gates in a conventional hybridization reaction.

While the "slow" F2 curves in Figure 2 roughly follow second order kinetics, the signaling reaction obtained for the DNA input at a 21.5 nm gate distance appears to contain a fast initial phase followed by a slow phase with similar kinetics as for the larger gate distances. This indicates that in this case at least a fraction of the signaling strands is transferred locally, "on-platform", from input gate 1 to output gate 2. As will be discussed below, the most likely cause for this effect is a direct physical interaction of the gates at this distance, which allows local strand transfer through some intermediary complex (*cf.* Figures 6, S9 (SI)). Interestingly, such a local transfer does not appear to be possible for the RNA input at the same gate distance. In contrast to the DNA case, upon hybridization of RNA input to gate 1, a slightly shorter A-form helical section (with $\approx$0.24$-$0.28 nm/bp[30,31] as opposed to 0.34 nm/bp in B-DNA) with sequence b/b* will be formed. Conceivably, this prevents a direct physical interaction of gate 1 and gate 2. Alternatively, the more strongly binding RNA input may displace signal strand from gate 1 more effectively, and thus preclude the formation of an intermediate complex. We also investigated the situation in which the protection strand is not displaced from gate 1. As before, the kinetics of the signal release step is independent of the distance between the gates. With P still bound to Q1, however, strand displacement of the output strand is considerably slowed down (Figure S10 (SI)). Additional gel electrophoresis experiments confirmed that the DSD cascade reactions were immobilized and took place on the origami structures (Figure S11 (SI)).

Robustness of the DSD Cascade. In order to further test the hypothesis of a "local transfer" of signal strands, we performed a series of competition experiments with origami-supported cascades for the different input-output distances, using DNA inputs. In these experiments, an increasing amount of competitor strands was added to the solution, which contained sequence domains a*$-$d* and were thus partially complementary to the signal strands (a potential release of signal strands by the competitor strands *via* strand invasion at the input gate was found to be negligible). We expected that a globally diffusing fraction of the signal strands would be affected by the presence of competitors more strongly than a potential "local" fraction (*cf.* Figure S12 (SI)). Indeed, as is shown in Figure 3 the release of output strands is almost completely suppressed for large amounts of competitor strands ($\approx$ 1 μM) for the 32 and 42.5 nm gate distances, whereas still a significant fraction of output is generated for the

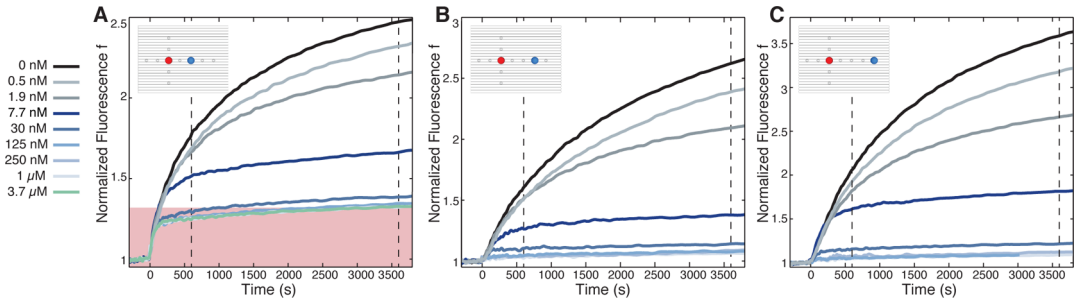

Figure 3. Probing strand transfer robustness with competitor strands partially complementary to the signal strands for distances (A) 21.5, (B) 32, (C) 42.5 nm. Fluorescence signals *f* are normalized to their respective starting values. The signal of the output fluorophore F2 is strongly affected by the interference with competitor strands. However, while the signal is completely suppressed for excessive competitor concentrations in (B) and (C), it remains finite for the shorter gate distance Δx = 21.5 nm in (A). The kinetics of the robust "local" signaling fraction (marked in red) is identical to that of the release process shown in Figure 2.

21.5 nm distance even at excessive competitor concentrations (3.7 μM). This is consistent with the assumption that the local transfer of signal strands for these distances occurs faster than hybridization with a competitor strand. Thus, colocalization at 21.5 nm not only speeds up the reaction and allows a fast local transfer of signal strands, but also significantly increases the robustness of the cascade with respect to a competing reaction pathway. This may be seen as a "dynamic" robustness as opposed to the "static" robustness of the larger gate distances with respect to intraorigami leakage.

We may interpret the fraction of signal *f* in Figure 3A that cannot be suppressed by the addition of competitor strands (marked in red) as caused by the locally transferred signaling strands. We can thus define a strand transfer efficiency η as a function of competitor strands $\eta([C]) = (f([C]) - 1)/(f(0) - 1)$. The locally transferred fraction then corresponds to the value η_∞ for long times and at excessive competitor concentrations. In fact, the kinetics of this fraction alone is identical to that of the release step (*cf.* Figure 2), which indicates that for the local signaling process input binding is rate-limiting.

Redundant Receiver Gates. The overall performance of the cascade can be further improved by introducing redundant receiver gates on the origami platforms. A larger number of colocalized targets is expected to increase the probability of transferring signal strands locally and thus decrease the diffusive loss of signals to the bulk. For the competition experiment shown in Figure 4, four copies of gate 2 were immobilized on the DNA origami platform, each ≈21.5 nm apart from the sender gate 1. Compared to the case of a single receiver gate at the same distance, the kinetics appears to be faster and the displacement of the output strand O shows a fast convergence to the maximum fluorescence level of F2. Moreover, the larger number of receiver gates seems to further increase the robustness of the cascade with respect to high competitor strand concentrations. As before, a similar experiment for the 10.5 nm gate distance was corrupted by excessive

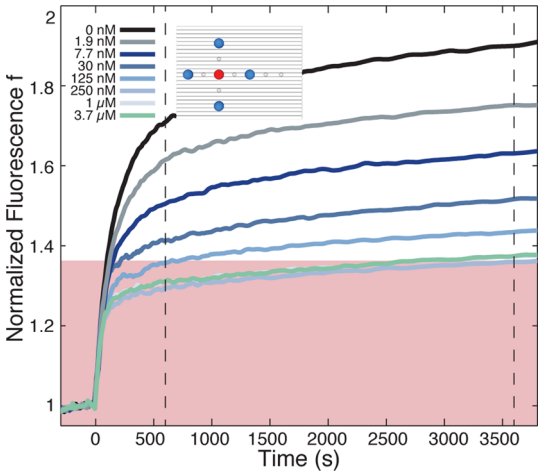

Figure 4. A competitor strand assay as in Figure 3 performed for a cascade with four receiver gates at a distance $\Delta x \approx$ 21.5 nm. In terms of the "surviving" signal strand fraction transferred even in the presence of excessive competitor strands, the redundant cascade is more robust.

leakage already during the preparation of the cascade, while additional receivers at 32 nm distance did not show any effect.

In Figures 3 and 4, relative fluorescence values normalized to the initial fluorescence are displayed rather than the reaction progress ξ defined above. It can be seen that in the absence of competitor strands the overall fluorescence increase is highest for the larger distances, whereas it is lowest for the multiple receiver case. This is caused by the correspondingly higher starting fluorescence values for the shorter distances (*cf.* Figure S5 (SI)), which in turn results from intraorigami leakage during preparation and purification. Furthermore, due to the presence of four (partially quenched) fluorophores F2 in Figure 4 the relative change with respect to the initial value is smaller.

A summary of the competition experiments is shown in Figure 5, where the transfer efficiencies $\eta([C])$ defined above are compared for the various cascade geometries at two different time points. The higher dynamic robustness of the shorter gate distance is

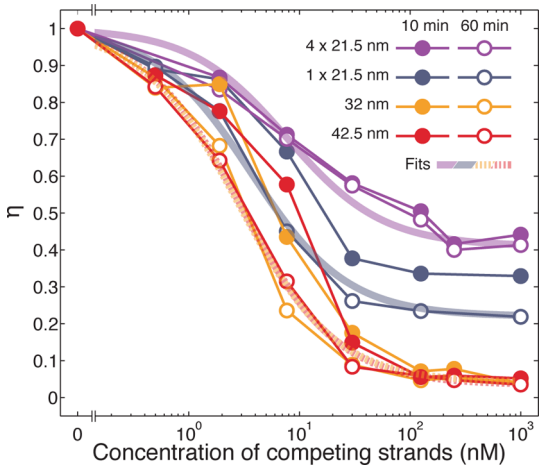

Figure 5. Effect of competing strands on the efficiency of signal transfer for the different distances and spatial arrangements on the DNA origami platform. η is defined as the relative fluorescence increase *f*-1 in the presence of competitor strands normalized to the undisturbed signal at the same time point (η is shown here for $t = 10$ min and $t = 60$ min to also capture kinetic effects). Signal transfer is most efficient for the 21.5 nm gate distance. In the redundant case (with four receiver gates), η is constant after 10 min. The thick, continuous lines display the theoretically expected reduction of η at long times with increasing competitor concentration. The curves are fits of the simple competition model described in the text to the "long term" values η ($t = 60$ min). The corresponding fit parameters were $\eta_\infty = 0.4, 0.2, 0, 0$ and $\gamma = 0.13, 0.27, 0.34, 0.33$ nM^{-1} for the 4 × 21.5, 1 × 21.5, 32, and 42.5 nm case, respectively.

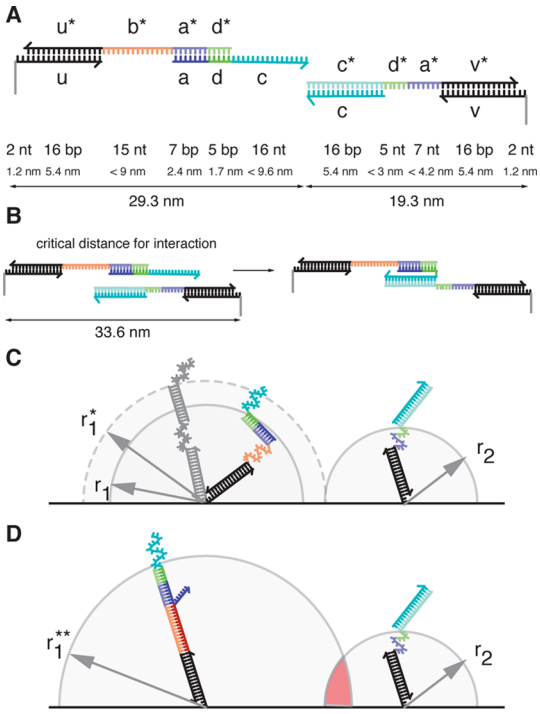

Figure 6. Geometric considerations: (A) The two gate complexes and their respective sequence domains. Fully stretched gate 1 would extend by 29.3 nm, while gate 2 would have a length of 19.3 nm (using 0.34 nm/bp for dsDNA and 0.6 nm/nt for ssDNA). (B) Direct interaction between the gates is only possible below a gate distance of ≈33.6 nm (assuming the unlikely case where both gate complexes are fully extended and lie horizontally on the origami platform); at this distance the sequence domains d/d* of both gates can "touch each other" and therefore signal strand S can assume an orientation in which it can displace the output strand on gate 2. (C) In a typical situation, the single-stranded sections will be relaxed, and thus gate extensions will be smaller than in the extreme cases of A and B. In a relaxed conformation, in which the dsDNA sections of gate 1 are colinear (shown in gray), the extension up to sequence domain d would be $r_1^* = 14.5$ nm. In general, however, the two duplexes will be randomly oriented, and the root-mean-square extension will be only $r_1 \approx 8.7$ nm. The extension of gate 2 (again up to domain d*) will be $r_2 \approx 7.5$ nm. (D) Hybridization of DNA input to gate 1 stretches the gate complex ($r_1^{**} = 15.8$ nm) and thus strongly enhances the interaction between the gates for the 21.5 nm distance. For an RNA input, $r_1^{**} = 14.3-14.9$ nm.

clearly reflected. Specifically, for the redundant cascade geometry with four output gates at $\Delta x \approx 21.5$ nm, more than $\eta = 40\%$ of the available signal strands are transferred even in the presence of excessive concentrations of interfering strands. In terms of η, there is essentially no difference between the 32 nm and the 42.5 nm gate distance.

The efficiency of signal transfer in the presence of competitor strands is expected to scale with their concentration [*C*] as

$$\eta([C]) = \eta_\infty + \frac{1-\eta_\infty}{1+\gamma[C]}$$

where $\gamma = k_c/k_{on}[O]$ is determined by the ratio of the reaction rates between sender and competitor strands k_c, the rate k_{on} for hybridization on the origami platforms and their concentration [*O*]. As can be seen in Figure 5, the measured values for η at $t = 60$ min (which approximate the long-term equilibrium values) follow this behavior very well.

DISCUSSION

Our experiments demonstrate that colocalization of components of a DNA strand displacement cascade onto a DNA origami platform has a strong effect on its performance for small gate distances. For the shortest distance investigated in this study, 10.5 nm, the direct physical overlap of the DSD gates (with comparatively large dimensions around ≈20 nm) leads to excessive strand displacement interactions already in the absence of input strands. This makes a stable preparation of a defined initial state of the cascade virtually impossible. Leak reactions presumably proceed *via* fraying of duplex ends followed by strand invasion of complementary sequence domains of neighboring DNA gates (Figures 6 and S9 (SI)). In solution such processes only occur very slowly (with a displacement rate of order 1−10 M^{-1} s^{-1} [32]), but their rate is significantly enhanced due to the huge effective concentrations of the reactants on the origami platform. The mean distance between reactants with a molar concentration *c* is $d = (c \cdot N_A)^{-1/3}$ which is ≈0.7 μm at $c = 5$ nM (N_A is Avogadro's constant). Thus, the distance between sender and receiver gates on the origami platforms is more than an

order of magnitude smaller, corresponding to an increase in local concentration by a factor of 2×10^5 for $\Delta x = 10.5$ nm (and still 3×10^4 for $\Delta x = 21.5$ nm). This situation is quite analogous to the speed-up of unfavorable reactions in DNA-templated synthesis.[18,33]

While for large distances (32, 42.5 nm in this study), a stable preparation of an initial state is possible, colocalization in this case does not provide any kinetic advantage, and the DSD cascade proceeds with a similar speed as in a diffusion-controlled bulk reaction. In our experiments, an overall beneficial effect of colocalization is only observed for an intermediate gate distance of ≈21.5 nm, for which enhanced kinetics of the cascade reaction and an increased robustness with respect to interference by a competitive reaction is found. Our experiments suggest that for the 21.5 nm gate distance signal strands are transferred locally from gate 1 to gate 2 of the same platform. A variety of scenarios for this local transfer are possible. As shown in Figure 6, already in the initial state gate 1 and gate 2, stretched to their contour lengths, can interact slightly. However, the single-stranded sections (b* on gate 1 and a*d* on gate 2) will be collapsed and an excursion to large extensions is improbable. Hybridization of input I to gate 1 renders the gate complex into a full duplex with larger (mean) extension, and thus the probability of interaction between the gates increases. At this point gate 1 and gate 2 may form an intermediate complex, in which signal S is "spooled over" without ever completely detaching from the origami platform. As indicated in Figure S9 (SI), such a transfer can happen in a variety of different ways, which cannot be distinguished in our experiments.

Alternatively, strand S could be completely displaced by the input, and then "locally diffuse" to the adjacent target gate. The efficiency of such a process depends on the ratio of the diffusion and the reaction time-scale. Assuming a diffusion coefficient for the 28 nt long signal strand S of order $D \approx 100\ \mu m^2/s$, a typical time-scale associated with diffusive processes over a distance Δx is given by $t_D \sim \Delta x^2/D$, which is only 1 μs for $\Delta x = 100$ nm, and 40 ns for $\Delta x = 20$ nm. Hence, a released signal strand will quickly explore its neighborhood on the origami platform by diffusion and also quite likely bump into a receiver gate.[34] DNA hybridization, however, is not diffusion-limited and occurs at a considerably slower time-scale,[35,36] and thus most of the encounters between signal and gate will not result in the successful nucleation of a helix.

Also the fact that an RNA input, resulting in only a slightly shorter input−gate 1 complex than the DNA input, does not speed up the cascade reaction disagrees with a "local diffusion" scenario (which should be more or less the same for DNA and RNA inputs), and thus supports a local strand transfer, which requires a direct physical linkage between gate 1 and gate 2.

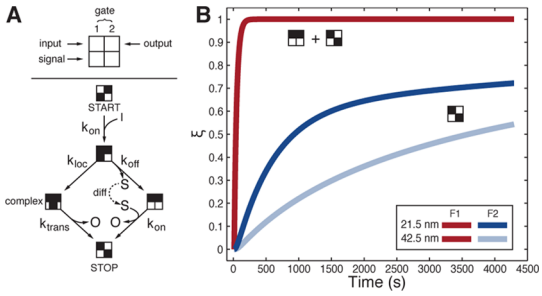

Figure 7. Simplified kinetic model of the cascade. (A) Schematic illustration of the gate composition and the dominant pathways that occur after binding of the input strand. (B) Simulated kinetic curves for gate distances of 21.5 and 42.5 nm. Rate constants are $k_{on} = 5.7 \times 10^4\ M^{-1}\ s^{-1}$, $k_{off} = 5.3 \times 10^3\ s^{-1}$, $k_{trans} = 0.0017\ s^{-1}$ for all curves and $k_{loc} = 7.6 \times 10^3\ s^{-1}$ for the shorter and $k_{loc} = 0\ s^{-1}$ for the larger distance.

Regardless of the microscopic details of the "on-platform" transfer, we can phenomenologically summarize the reactions involved in the DSD cascade in the simplified kinetic scheme displayed in Figure 7 (for modeling and parameter estimation see Supporting Information). In this scheme, binding of an input strand to an origami platform (with rate k_{on}) sets gate 1 into an "activated state". From this, signal strand S can either detach by spontaneous dissociation of the 5 bp d/d* duplex (rate k_{off}), or create an intermediate complex with gate 2 (rate k_{loc}). From this complex, signal strand is transferred completely to gate 2 with rate k_{trans}, accompanied by the release of output strand (which is not included explicitly in the model as it is not rate-limiting here). Alternatively, strands S released to the bulk rebind to available origami platforms in a conventional hybridization reaction (again with rate k_{on}). As can be seen from the simulated kinetic curves in Figure 7, this model captures the experimental observations from Figure 2 very well using realistic parameter settings. Specifically, the fitted $k_{on} = 5.7 \times 10^4\ M^{-1}\ s^{-1}$ agrees very well with the rough estimate based on $t_{1/2}$ above, and $k_{off} = 5.3 \times 10^3\ s^{-1}$ corresponds well with an off-rate expected for a 5 bp duplex. $k_{trans} = 0.0017\ s^{-1}$ indicates that the transfer event itself is relatively slow. The fraction of locally transferred strands $k_{loc}/k_{loc} + k_{off} \approx 59\%$ in the model is larger than that estimated from the competition experiments (*i.e.*, η_∞), which indicates that competitor strands might interfere also with local transfer processes.

CONCLUSION

We have shown that localization on an origami platform influences the performance of a DNA strand displacement cascade in various ways. For very small distances, at which the stages of the cascade are in direct physical contact, preparation of the cascade constructs is corrupted by strong intraorigami leak reactions. For distances at which the DSD gates are well separated there is no leak, but also no benefit of colocalization. The cascade reaction is sped up for intermediate distances, at which the two gates just barely interact with each

other in the absence of an input strand. Hybridization of input and sender gate presumably improves the overlap between sender and receiver and facilitates the formation of an intermediate complex, in which the signal strand is spooled over from its start to its end position. Most importantly, this type of localized signal transfer makes the cascade reaction robust with respect to excessive amounts of complementary interfering strands in solution, which may be important for utilization of similar mechanisms in complex environments, or when running several alternative processes in parallel.

Our findings also suggest that the performance of the cascade could be optimized by fine-tuning the distances between the gates, and also by deliberately utilizing length and conformational changes that reduce or increase the interaction between neighboring gates. As a complete release of intermediate strands is not desirable, all strands comprising a circuit would have to be kept immobilized on the platform all the time, and in this sense an immobilized signaling cascade would not differ considerably from DNA walker or motor systems.[9,16,37−41]

A different gate architecture with improved strand design and using protective secondary structures could reduce leak reactions and thus facilitate smaller gate distances. Some of the leak occurring after deprotection of the DSD cascade could potentially be avoided by "clamping" the c domain in a similar manner as previously demonstrated by Qian and Winfree for seesaw gates,[8] which strongly reduced undesired strand invasion reactions. Conceivably, however, introduction of more stable secondary structures would diminish the kinetic advantage conveyed by colocalization in the first place. An alternative would be to simply take leakage into account in the design of the cascades and dynamically assemble or disassemble the gates on the platforms "on the fly", *i.e.*, during operation of the circuits. The challenge is to create kinetic pathways in which desirable processes occur at a much faster rate than undesired ones.

MATERIALS AND METHODS

Assembly of the DNA Origami Structures. DNA origami structures were designed using caDNAno 2 (*cf.* Figure S1a (SI)).[42] A 7249 nt long DNA sequence derived from the genome of the bacteriophage M13 (M13mp18) was used as scaffold (kindly provided by the group of H. Dietz, TUM).[43] Extended staple strands and dye modified oligonucleotides were purchased from Biomers, Ulm, Germany. All sequences and modifications are listed in the final section of the Supporting Information. The DNA origami structures were folded in a one pot thermal annealing reaction (from 70 to 40 °C at a rate of 0.5 °C/min) at 48 nM scaffold concentration and 200 nM (4× molar excess over the scaffold) for each structural staple and 400 nM (8× molar excess) for extended staples, which were used for the attachment of the gates of the cascade. Staples at the short edges of the origami structures were left out to prevent blunt-end stacking. The folding buffer contained 12.5 mM $MgCl_2$ and 1× TAE (40 mM Tris, 20 mM acetic acid, 1 mM EDTA, pH 8.0) and was also used for further sample preparation. The origami design is based on a regular rectangle origami structure,[25] which was twist corrected to ensure a planar structure (tcRRO). Unmodified staple strands were purchased at MWG Eurofins Genomics, Ebersberg, Germany. For purification of the folded origami structures, PEG precipitation was applied as described previously.[44] The desired concentration of the tcRRO was measured by a spectrophotometer.

Preparation of the DSD Gates. Previous to attachment to the extended staples of the DNA origami structure, the two dye modified DNA gate complexes constituting the DNA signaling cascade were hybridized separately at room temperature in folding buffer (see above) for at least 1 h. Gate 1 of the cascade was constructed of three strands, a fluorophore-labeled strand (labeled with F1 = Atto647N), the signal strand S (labeled with quencher Q1 = BBQ-650), and a protective DNA strand (P), which served to reduce undesirable strand displacement reactions during the assembly. The concentrations for F1, S and P were 3, 4.5, 7.5 μM, respectively. Gate 2 was composed of a gate strand labeled with fluorophore F2 (Atto532) and output strand O (labeled with quencher Q2 = BHQ-1), which were incubated at concentrations of 3 μM and 6 μM, respectively. The assembly procedure is shown in Figure S2 (SI).

Attachment of the Fluorophore and Quencher Pairs to the DNA Origami Platform. The purified DNA origami structures were first incubated with F1-Q1-P in 2× excess for 1 h at room temperature. The construct was subsequently purified by PEG precipitation, which was repeated for two times. Afterward, F2-Q2 was incubated with the DNA origami structures in 1.5× excess for 20 min at room temperature, which in turn was again purified 2 times by PEG purification. Finally, the protective DNA strand P was removed by its complementary sequence P* (domains z* and c) in 3× excess and an incubation for 1 min. The sample was diluted to 5 nM in folding buffer and stored in aliquots at −80 °C.

Preparation of Serial Dilutions of Competitor Strands. Synthetic DNA and RNA analogs of miRNA-21 (DNA-21, RNA-21 ordered from Biomers, Ulm, Germany), served as input signals for the cascade. Their concentration was initially set to 10.7 μM. Serial dilutions of competitor strands were performed as follows: 25 μL of 100 μM competitor strand was mixed with 75 μL of 1× TAE buffer, 12.5 mM $MgCl_2$. 50 μL of this dilution was subsequently diluted with 50 μL of folding buffer. This dilutive step was repeated 12 times. After dilution, the competitor strand solutions were mixed with 6 μL of 100 μM DNA-21 and stored at 4 °C.

Fluorescence Spectroscopy. Fluorescence spectroscopy experiments were carried out with a Cary Eclipse spectrometer (Agilent Technologies Deutschland GmbH, Böblingen, Germany). The Atto 532 dye (F2) was excited at 532 ± 10 nm and observed at 554 ± 10 nm, while Atto 647N (F1) was excited at 647 ± 10 nm and observed at 669 ± 10 nm. For each experiment 65 μL of sample was filled into fluorescence cuvettes (105.254-QS, Hellma GmbH & Co. KG, Müllheim, Germany). All measurements were performed at 20 °C. For kinetic measurements, 3 μL of input strand were added to a 65 μL sample. Rapid mixing was achieved by carefully but quickly pipetting up and down the whole volume for several times without generation of bubbles or loss of material.

Atomic Force Microscopy. Imaging of individual gates using atomic force microscopy (AFM) was carried out with an Asylum Research Cypher scanning probe microscope (Figure S1B (SI)). Because of the flexibility of the gate complexes, individual gate positions could only be imaged after hybridization of biotin functionalized oligonucleotides and subsequent labeling with streptavidin. For biotinylation, DNA origami structures were folded as described above. After incubation with biotinylated oligonucleotides (60 min) the sample was purified and diluted to 2.5 nM in folding buffer. Five μL of origami solution were added to a freshly cleaved mica surface. After addition of 60 μL of folding buffer, 2 μL of 500 nM streptavidin solution was added to the droplet. Imaging was carried out in liquid AC mode with an Olympus microcantilever BL-AC40TS-C2.

Gel Electrophoresis. For the analysis of successful folding and immobilization of the gates, the samples were electrophoresed in an agarose gel. 1% of agarose was dissolved in folding buffer. 24 μL of 5 nM purified origami platforms were mixed with 5 μL of 40% sucrose and subsequently loaded into the gel chambers. The gel was run at 100 V for 1.5 h in an ice cooled water bath. The gel was analyzed using a laser scanner (Typhoon FLA 9500) with excitation at 532 nm. Subsequently, the gel was stained with SybrGold and imaged again.

Conflict of Interest: The authors declare no competing financial interest.

Acknowledgment. The authors gratefully acknowledge funding by the Deutsche Forschungsgemeinschaft (SFB 1032/TP A2 and Nanosystems Initiative Munich). We kindly thank Florian Praetorius for supplying the M13mp18 scaffold.

Supporting Information Available: Supporting Figures S1–S12 and oligonucleotide sequences. This material is available free of charge *via* the Internet at http://pubs.acs.org.

REFERENCES AND NOTES

1. Zhang, D. Y.; Seelig, G. Dynamic DNA Nanotechnology Using Strand-Displacement Reactions. *Nat. Chem.* **2011**, *3*, 103–113.
2. Yurke, B.; Mills, A. Using DNA to Power Nanostructures. *Genet. Program. Evolvable Mach.* **2003**, *4*, 111–122.
3. Zhang, D. Y.; Winfree, E. Control of DNA Strand Displacement Kinetics Using Toehold Exchange. *J. Am. Chem. Soc.* **2009**, *131*, 17303–17314.
4. Srinivas, N.; Ouldridge, T. E.; Sulc, P.; Schaeffer, J. M.; Yurke, B.; Louis, A. A.; Doye, J. P. K.; Winfree, E. On the Biophysics and Kinetics of Toehold-Mediated DNA Strand Displacement. *Nucleic Acid Res.* **2013**, *41*, 10641–10658.
5. Phillips, A.; Cardelli, L. A Programming Language for Composable DNA Circuits. *J. R. Soc., Interface* **2009**, *6*, S419–S436.
6. Krishnan, Y.; Simmel, F. C. Nucleic Acid Based Molecular Devices. *Angew. Chem., Int. Ed.* **2011**, *50*, 3124–3156.
7. Seelig, G.; Soloveichik, D.; Zhang, D. Y.; Winfree, E. Enzyme-Free Nucleic Acid Logic Circuits. *Science* **2006**, *314*, 1585–1588.
8. Qian, L.; Winfree, E. Scaling up Digital Circuit Computation with DNA Strand Displacement Cascades. *Science* **2011**, *332*, 1196–1201.
9. Yin, P.; Choi, H. M.; Calvert, C. R.; Pierce, N. A. Programming Biomolecular Self-Assembly Pathways. *Nature* **2008**, *451*, 318–322.
10. Zhang, D. Y.; Turberfield, A. J.; Yurke, B.; Winfree, E. Engineering Entropy-Driven Reactions and Networks Catalyzed by DNA. *Science* **2007**, *318*, 1121–1125.
11. Qian, L.; Winfree, E.; Bruck, J. Neural Network Computation with DNA Strand Displacement Cascades. *Nature* **2011**, *475*, 368–372.
12. Rinaudo, K.; Bleris, L.; Maddamsetti, R.; Subramanian, S.; Weiss, R.; Benenson, Y. A Universal RNAi-Based Logic Evaluator That Operates in Mammalian Cells. *Nat. Biotechnol.* **2007**, *25*, 795–801.
13. Wang, D.; Fu, Y.; Yan, J.; Zhao, B.; Dai, B.; Chao, J.; Liu, H.; He, D.; Zhang, Y.; Fan, C.; Song, S. Molecular Logic Gates on DNA Origami Nanostructures for MicroRNA Diagnostics. *Anal. Chem.* **2014**, *86*, 1932–1936.
14. Chandran, H.; Gopalkrishnan, N.; Phillips, A.; Reif, J. Localized Hybridization Circuits. In *DNA Computing and Molecular Programming*; Cardelli, L., Shih, W., Eds.; Springer: Berlin, 2011; Vol. 6937, pp 64–83.
15. Muscat, R. A.; Strauss, K.; Ceze, L.; Seelig, G. DNA-Based Molecular Architecture with Spatially Localized Components. In *Proceedings of the 40th Annual International Symposium on Computer Architecture*; ACM: Tel-Aviv, Israel, 2013; pp 177–188.
16. Dannenberg, F.; Kwiatkowska, M.; Thachuk, C.; Turberfield, A. DNA Walker Circuits: Computational Potential, Design, and Verification. In *DNA Computing and Molecular Programming*; Soloveichik, D., Yurke, B., Eds.; Springer International Publishing: Berlin, 2013; Vol. 8141, pp 31–45.
17. Conrado, R. J.; Varner, J. D.; DeLisa, M. P. Engineering the Spatial Organization of Metabolic Enzymes: Mimicking Nature's Synergy. *Curr. Opin. Biotechnol.* **2008**, *19*, 492–499.
18. Li, X.; Liu, D. R. DNA-Templated Organic Synthesis: Nature's Strategy for Controlling Chemical Reactivity Applied to Synthetic Molecules. *Angew. Chem., Int. Ed.* **2004**, *43*, 4848–4870.
19. He, Y.; Liu, D. R. Autonomous Multistep Organic Synthesis in a Single Isothermal Solution Mediated by a DNA Walker. *Nat. Nanotechnol.* **2010**, *5*, 778–782.
20. Niemeyer, C. M.; Koehler, J.; Wuerdemann, C. DNA-Directed Assembly of Bienzymic Complexes from *in Vivo* Biotinylated NAD(P)H: FMN Oxidoreductase and Luciferase. *ChemBioChem* **2002**, *3*, 242–245.
21. Wilner, O. I.; Weizmann, Y.; Gill, R.; Lioubashevski, O.; Freeman, R.; Willner, I. Enzyme Cascades Activated on Topologically Programmed DNA Scaffolds. *Nat. Nanotechnol.* **2009**, *4*, 249–254.
22. Muller, J.; Niemeyer, C. DNA-Directed Assembly of Artificial Multienzyme Complexes. *Biochem. Biophys. Res. Commun.* **2008**, *377*, 62–67.
23. Fu, J.; Liu, M.; Liu, Y.; Woodbury, N. W.; Yan, H. Interenzyme Substrate Diffusion for an Enzyme Cascade Organized on Spatially Addressable DNA Nanostructures. *J. Am. Chem. Soc.* **2012**, *134*, 5516–5519.
24. Fu, Y.; Zeng, D.; Chao, J.; Jin, Y.; Zhang, Z.; Liu, H.; Li, D.; Ma, H.; Huang, Q.; Gothelf, K. V.; Fan, C. Single-Step Rapid Assembly of DNA Origami Nanostructures for Addressable Nanoscale Bioreactors. *J. Am. Chem. Soc.* **2013**, *135*, 696–702.
25. Rothemund, P. W. K. Folding DNA to Create Nanoscale Shapes and Patterns. *Nature* **2006**, *440*, 297–302.
26. Lu, J.; Getz, G.; Miska, E.; Alvarez-Saavedra, E.; Lamb, J.; Peck, D.; Sweet-Cordero, A.; Ebet, B.; Mak, R.; Ferrando, A.; Downing, J.; Jacks, T.; Horvitz, H.; Golub, T. MicroRNA Expression Profiles Classify Human Cancers. *Nature* **2005**, *435*, 834–838.
27. Volinia, S.; Calin, G.; Liu, C.; Ambs, S.; Cimmino, A.; Petrocca, F.; Visone, R.; Iorio, M.; Roldo, C.; Ferracin, M.; Prueitt, R.; Yanaihara, N.; Lanza, G.; Scarpa, A.; Vecchione, A.; Negrini, M.; Harris, C.; Croce, C. A MicroRNA Expression Signature of Human Solid Tumors Defines Cancer Gene Targets. *Proc. Natl. Acad. Sci. U. S. A.* **2006**, *103*, 2257–2261.
28. Dessinges, M.-N.; Maier, B.; Zhang, Y.; Peliti, M.; Bensimon, D.; Croquette, V. Stretching Single Stranded DNA, a Model Polyelectrolyte. *Phys. Rev. Lett.* **2002**, *89*, 248102.
29. Murphy, M.; Rasnik, I.; Cheng, W.; Lohman, T.; Ha, T. Probing Single-Stranded DNA Conformational Flexibility Using Fluorescence Spectroscopy. *Biophys. J.* **2004**, *86*, 2530–2537.
30. Dickerson, R. E.; Drew, H. R.; Conner, B. N.; Wing, R. M.; Fratini, A. V.; Kopka, M. L. The Anatomy of A-, B-, and Z-DNA. *Science* **1982**, *216*, 475–485.
31. Milman, G.; Langridge, R.; Chamberlin, M. J. The Structure of a DNA-RNA Hybrid. *Proc. Natl. Acad. Sci. U. S. A.* **1967**, *57*, 1804–1810.
32. Reynaldo, L. P.; Vologodskii, A. V.; Neri, B. P.; Lyamichev, V. I. The Kinetics of Oligonucleotide Replacements. *J. Mol. Biol.* **2000**, *297*, 511–520.
33. Hansen, M. H.; Blakskjaer, P.; Petersen, L. K.; Hansen, T. H.; Hojfeldt, J. W.; Gothelf, K. V.; Hansen, N. J. V. A Yoctoliter-Scale DNA Reactor for Small-Molecule Evolution. *J. Am. Chem. Soc.* **2009**, *131*, 1322–1327.
34. Berg, H. C. *Random Walks in Biology*; Princeton University Press: Princeton, NJ, 1993.
35. Pörschke, D.; Eigen, M. Co-Operative Non-Enzymic Base Recognition. 3. Kinetics of the Helix-Coil Transition of the Oligoribouridylic–Oligoriboadenylic Acid System and of Oligoriboadenylic Acid Alone at Acidic pH. *J. Mol. Biol.* **1971**, *62*, 361–381.
36. Craig, M.; Crothers, D.; Doty, P. Relaxation Kinetics of Dimer Formation by Self Complementary Oligonucleotides. *J. Mol. Biol.* **1971**, *62*, 383–401.
37. Tian, Y.; He, Y.; Chen, Y.; Yin, P.; Mao, C. A Dnazyme That Walks Processively and Autonomously Along a One-Dimensional Track. *Angew. Chem., Int. Ed.* **2005**, *44*, 4355–4358.

38. Green, S.; Bath, J.; Turberfield, A. Coordinated Chemomechanical Cycles: A Mechanism for Autonomous Molecular Motion. *Phys. Rev. Lett.* **2008**, *101*, 238101.
39. Omabegho, T.; Sha, R.; Seeman, N. C. A Bipedal DNA Brownian Motor with Coordinated Legs. *Science* **2009**, *324*, 67–71.
40. Lund, K.; Manzo, A. J.; Dabby, N.; Michelotti, N.; Johnson-Buck, A.; Nangreave, J.; Taylor, S.; Pei, R.; Stojanovic, M. N.; Walter, N. G.; Winfree, E.; Yan, H. Molecular Robots Guided by Prescriptive Landscapes. *Nature* **2010**, *465*, 206–210.
41. Wickham, S. F. J.; Endo, M.; Katsuda, Y.; Hidaka, K.; Bath, J.; Sugiyama, H.; Turberfield, A. J. Direct Observation of Stepwise Movement of a Synthetic Molecular Transporter. *Nat. Nanotechnol.* **2011**, *6*, 166–169.
42. Douglas, S. M.; Marblestone, A. H.; Teerapittayanon, S.; Vazquez, A.; Church, G. M.; Shih, W. M. Rapid Prototyping of 3D DNA-Origami Shapes with Cadnano. *Nucleic Acid Res.* **2009**, *37*, 5001–5006.
43. Douglas, S. M.; Dietz, H.; Liedl, T.; Högberg, B.; Graf, F.; Shih, W. M. Self-Assembly of DNA into Nanoscale Three-Dimensional Shapes. *Nature* **2009**, *459*, 414–418.
44. Douglas, S. M.; Chou, J. J.; Shih, W. M. DNA-Nanotube-Induced Alignment of Membrane Proteins for NMR Structure Determination. *Proc. Natl. Acad. Sci. U. S. A.* **2007**, *104*, 6644–6648.